Layer by layer solidification of ^{4}He in narrow porous media

M. Rossi, D. E. Galli, and L. Reatto
Dipartimento di Fisica, Università degli Studi di Milano, via Celoria 16, 20133 Milano, Italy
(Received 6 May 2005; published 18 August 2005)

We give a variational Monte Carlo description of ^{4}He filling under pressure a porous material modeled by a smooth cylindrical nanopore. Our trial wave function is a shadow wave function which allows different degrees of correlation between ^{4}He atoms depending on the distance from the pore wall but still preserving the full Bose symmetry. The radial density profile shows a strong layering of the ^{4}He atoms which are located in concentric annuli. This system has a very rich phase diagram with at least four different phases. The layer in contact with the pore is always solid. For our narrow pore radius ($R=13$ Å), as the density is increased, solidification takes place layer by layer, starting from the pore wall, as is confirmed by the static structure factors. The pore radius is too small to allow a bulklike solid to nucleate in the liquid region at the center of the pore, and in order to have a complete crystalline order in all the layers a pressure greater than 200 bar is needed. Computing the one body density matrix we are able to estimate the condensate fraction, which is still nonzero even if all the layers are in the solid phase.

DOI: 10.1103/PhysRevB.72.064516 PACS number(s): 67.80.Mg, 67.90.+z, 67.40.Db

I. INTRODUCTION

The behavior of helium confined in restricted geometry is a topic of current interest in quantum physics. It is known that the interplay of the confining potential with the interparticle interaction may yield completely new phenomena, as well as strongly enhancing correlations effects: ^{4}He adsorbed in porous media is an excellent example of a confined interacting Bose system. The properties of liquid ^{4}He in several porous media have been extensively investigated with a considerable experimental[1–6] and theoretical[7–10] effort over the past years. The reduced dimensionality induces remarkable effects on the properties of ^{4}He modifying the phase diagram. For example, the confinement tends to inhibit freezing, so that pressures substantially higher than in the bulk are required for solidification, and the superfluidity is slightly suppressed.[1–3]

Much attention has been experimentally given also to the properties of pressurized ^{4}He in such geometries because of the possible existence of a supersolid phase. Flow without dissipation is intuitively associated with the liquid phase, but the presence of delocalized vacancies and defects, due to quantum mechanical fluctuations, can in principle allow the appearance of superfluidity in the solid.[11,12] Solid helium configuration in porous media is richer of vacancies and disorder than the bulk, so these systems stand for good candidates for observing a supersolid state. In a recent torsional oscillator experiment with solid ^{4}He confined in Vycor,[13] an abrupt drop in the rotational inertia has been observed below a certain critical temperature, which has been interpreted with the presence of a supersolid phase. However, a supersolid response has been also observed in the pure bulk solid ^{4}He[14] so that the role of defects is not clear at the present time.

It was observed that, for ^{4}He adsorbed in porous materials, the critical temperature for the onset of superfluidity is lowered decreasing the pore size.[2] Very recently, the behavior of ^{4}He filling a porous media with narrow pores as Gelsil has been investigated by means of the torsional oscillator technique revealing some quite unexpected features.[5] Gelsil is a porous silica glass whose structure is characterized by a random network of nanopores, similarly to Vycor. The sample employed in the experiments described in Ref. 5 has a nominal pore diameter of 25 Å which is significantly smaller than the typical Vycor value of 70 Å. Even at very low temperature, when the pressure is increased, an anomalous suppression of the superfluid response takes place for a critical pressure P_c of about 35 bar, where ^{4}He has not completely solidified. The strong confinement due to the small size and the disorder of the pore structure are supposed to be responsible for the reduction of the superfluid transition temperature and of the superfluid density, but, in order to explain a possible continuous transition at $T=0$ K and $P=P_c$ from a superfluid to a nonsuperfluid state, the existence of a quantum phase transition has been supposed.[5] No indication of solidification was found during this experiment[5] for pressure up to 50 bar, and the nature of the nonsuperfluid state near the critical pressure has to be investigated to confirm the quantum phase transition scenario.[5]

In this paper we present a variational Monte Carlo study of the ground state properties of ^{4}He filling a porous media. Although there have been many calculations for ^{4}He in confined geometry,[7–10] to our knowledge, there are no microscopic calculations tackling the behavior of ^{4}He in a cylindrical confinement. In fact, some information on the superfluid fraction and the critical temperature are obtained extending the results for dilute Bose gas[15] or hard sphere gas[7] in random potentials. The equation of state has been studied confining helium in a lattice of big static objects with a purely repulsive interaction.[9] Results on the excitation spectrum are given for the liquid phase in a slit pore geometry[8] and, still in slit geometry, a very recent simulation[10] deals with the superfluid response of ^{4}He at 62 bar.

We have modeled the confining media with a long smooth cylindrical pore of radius $R=13$ Å, a size comparable with

the Gelsil pore size, and we have chosen the He-pore potential in order to represent the He-Si interaction. Our trial wave function is a shadow wave function (SWF),[16] which has been shown to be able to describe in an excellent way the properties of ^{4}He both in uniform and nonuniform states.[17–21] We find that ^{4}He forms a distinct layered structure with the atoms arranging themselves in concentric annuli and there is no bulklike solid in the center of our pore because of its reduced size. The atoms in the layer adjacent to the pore wall are very localized under all conditions of a filled pore, we call this the inert layer. Increasing the helium density a layer by layer solidification takes place starting from the layer closest to the inert layer. The computed static structure factors of these layers are compatible with a planar regular triangular lattice wrapped on a cylindrical surface, and pressures greater than 200 bar are needed in order to have solidification in the whole system. We have also studied the presence of Bose-Einstein condensation (BEC) by computing the one-body density matrix. By computing single layer contributions to the one-body density matrix we find BEC over an extended pressure range and, for the central layers, there is a nonzero condensate fraction up to pressure of the order of 270 bar when the whole system is in the solid phase.

The paper is organized as follows: in Sec. II we give a brief presentation of the SWF that we have employed, we describe our model for a silica porous glass and we give also some details of our simulations. Our results are reported and discussed in Sec. III. We analyze the microscopic structure of the system in terms of the radial density profiles and of the static structure factors, and, by computing the one-body density matrix, we give information also on the condensate fraction in the system. Section IV contains our conclusions.

II. MODEL AND SIMULATION METHOD

A. Shadow wave function

In a shadow wave function the atoms are correlated not only by standard direct correlations between particles, but also indirectly via the coupling to a set of subsidiary (shadow) variables. Integration over the shadow variables introduces effective interparticle correlations between pair of ^{4}He atoms but also between triplets and, in principle, to all orders in an implicit way; this is done so efficiently that it is possible to treat the liquid and the solid phase with the same functional form[18,20,22] without the need to introduce *a priori* equilibrium positions to localize the ^{4}He atoms around lattice positions. Solidification, in fact, emerges as a result of a spontaneously broken symmetry transition due to the increased correlations as the density of the system increases. The general form of a SWF is given by

$$\Psi(R) = \phi_r(R) \int dS \Theta(R,S) \phi_s(S), \tag{1}$$

where $R=(\mathbf{r}_1,\ldots,\mathbf{r}_N)$ and $S=(\mathbf{s}_1,\ldots,\mathbf{s}_N)$ are, respectively, the real and the shadow coordinates of the N ^{4}He atoms.

As usual with SWF, $\phi_r(R)$ is a Jastrow function and we assume a McMillan form pseudopotential,[22] while, for our system, $\phi_s(S)$ is the product of two terms. The first is the usual Jastrow function giving the intershadow correlation and as a pseudopotential we use the rescaled and shifted interatomic potential[22] chosen to be a standard Aziz potential.[23] In principle it is possible to reach a better variational description using a fully optimized SWF,[18] however we preferred the use of pseudopotentials with a smaller number of variational parameters due to the high number of particles imposed by the chosen model and the necessity to make simulations for a wide range of densities. The second term in $\phi_s(S)$ is a one-body term which represents the effect of the He-pore interaction. For the one-body pseudopotential we take the rescaled and shifted helium-pore potential. In this way, the correlations between the ^{4}He atoms and the pore wall are introduced via the shadow variables, and the simulation is simplified. The He-pore potential has a very deep attractive well compared to the He-He one. Therefore for the atoms closest to the wall we might expect a reduced zero point motion compared to that of atoms in the center of the pore. We allow for this effect by modifying the usual Gaussian kernel $\Theta(R,S)$ in the following way:[21]

$$\Theta(R,S) = \exp\left\{ -\sum_{i=1}^{N} \mathcal{C}(s_i^{xy}) |\mathbf{r}_i - \mathbf{s}_i|^2 \right\}, \tag{2}$$

where

$$\mathcal{C}(s_i^{xy}) = C + \Delta_C \left[1 - \exp\left(- \frac{(s_i^{xy}/r_0)^{2n}}{(s_i^{xy}/r_0)^2 + 1} \right) \right] \tag{3}$$

and $s^{xy}=\sqrt{(s^x)^2+(s^y)^2}$ is the radial distance from the cylinder axis, chosen to lie on the z direction, while $\{\Delta_C, r_0, n, C\}$ are variational parameters. The optimized parameters are obtained minimizing the expectation value of the Hamiltonian and are reported in Table I for few densities.

B. Helium-pore potential

We have chosen to model the confining media by a cylindrical nanopore and in order to resemble the Gelsil pore size we have fixed our pore radius at $R=13$ Å. We have assumed that the potential energy experienced by an ^{4}He atom can be evaluated by a summation over two-body interactions, chosen as isotropic Lennard-Jones (12,6), between the ^{4}He atom and the atoms composing the pore surface. Ignoring the atomistic details in the potential inside the pore by smearing out the pore surface atoms, the potential experienced by an ^{4}He atom at distance r from the axis of the cylinder is given by[24]

$$V(r,R) = 3\pi\gamma\varepsilon\sigma^2 \left[\frac{21}{32} \left(\frac{\sigma}{R} \right)^{10} M_{11}(x) - \left(\frac{\sigma}{R} \right)^4 M_5(x) \right], \tag{4}$$

where ε and σ are the LJ parameters for the interaction He pore, γ is the surface density of the atoms on the pore wall, R is the cylinder radius and $x=r/R$. Moreover M_n are special integrals

$$M_n(x) = \int_0^\pi d\phi \frac{1}{(1+x^2-2x\cos\phi)^{n/2}}. \tag{5}$$

We have employed as parameter values $\gamma\varepsilon=7.63$ K Å^{-2} and $\sigma=2.19$ Å chosen to represent the He-Si interaction.[25]

TABLE I. Optimized variational parameters for some effective densities: b and m are the McMillan parameters for $\phi_r(R)$; C, Δ_C, r_0, and n are the parameters for the Gaussian kernel $\Theta(R,S)$ as defined in (2); δ, α and δ', α' are, respectively, the rescale and shift parameters for the shadow-shadow and the shadow-pore pseudopotential in $\phi_s(S)$. The number N_{free} of free ^{4}He atoms in the simulation box, i.e., the total number of atoms minus the number of the inert layer, and the corresponding effective densities are also reported.

ρ_{eff} (Å^{-3})	N_{free}	b (Å)	m	C (Å^{-2})	Δ_C (Å^{-2})	r_0 (Å)	n	δ (K^{-1})	α	δ' (K^{-1})	α'
0.02400	138	2.78	5	0.78	4.5	9.6	4	0.04	0.98	0.235	1.04
0.03026	174	2.78	5	0.98	4.5	9.6	4	0.09	0.94	0.235	1.04
0.03478	200	2.80	5	0.92	4.5	9.6	4	0.10	0.94	0.235	1.04
0.03860	222	2.80	5	1.10	4.5	9.6	4	0.11	0.96	0.235	1.04
0.04070	234	2.82	5	1.10	4.5	9.6	4	0.11	0.96	0.235	1.04

The resulting ^{4}He-pore potential has an attractive well of −153 K at 2.2 Å from the pore wall and is plotted in Fig. 1. This single-pore model is more realistic than those employed in Refs. 8–10, but it still excludes effects due to the complex, highly networked geometry of porous glasses. It is possible to give a better description of the confining porous glass[26] studying fully networked system, but a realistic model even of a small chunk of the smallest-pore-networked glass might involve hundreds of thousands of atoms.

C. Simulation

We perform VMC simulations with a nanopore of radius $R=13$ Å and length $L=21.62$ Å, with periodic boundary conditions along the pore axis lying in the z direction, and with a number of ^{4}He atoms between $N=304$ and $N=403$, which corresponds to nominal densities from $\rho=0.0265$ Å^{-3} to $\rho=0.0351$ Å^{-3}, respectively. The actual density of ^{4}He atoms is 20% higher than the nominal value because not all the volume of the cylinder is available to ^{4}He atoms due to the strong He-wall repulsion; see Fig. 1. Because of the great number of particles and of the highly inhomogeneous state of the system very long equilibration runs are needed, so our simulation runs have never an equilibration shorter than 3×10^6 per particle Monte Carlo steps and the simulations run are in general 6×10^6 per particle Monte Carlo steps long. We find that the properties of the adsorbed layer at the pore wall are almost independent on the total density of the system. These atoms are localized and the interparticle distance corresponds, in bulk ^{4}He, to a density $\rho=0.047$ Å^{-3} and to a pressure $P=780$ bar.[27] This insensitivity of the adsorbed layer on the average density is similar to what was experimentally found for H_2 in Vycor.[28]

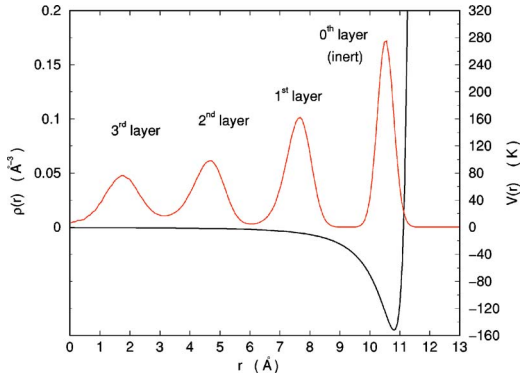

FIG. 1. (Color online) The pore-helium interaction potential for a $R=13$ Å pore and radial density profile at $\rho=0.03130$ Å^{-3} in a run in which all atoms are mobile.

The adsorbed layer in our cell contains 172 ^{4}He atoms, almost half of the particles in the system, at areal density of $n=0.12$ Å^{-2}. It is interesting to note that this is the critical coverage for the superfluidity onset for ^{4}He films in Gelsil.[5] For adsorbed films, the critical coverage corresponds to the value of n above which a superfluid film grows on the adsorbed layer, which is nonsuperfluid because of the strong van der Waals attraction from the glass wall. That this inert layer is nonsuperfluid has been confirmed theoretically by very recent path integral Monte Carlo (PIMC) simulation[10] for ^{4}He in a slit geometry for Vycor. Because of their great number and of the large value of their potential energy, the atoms of the inert layer tend to dominate the variational parameters optimization and to mask the contribution of the other layers to the equation of state, so we have chosen to fix the position of the atoms of the inert layer, treating them as a part of the substrate. It is worthy to note that this choice is not forced by our variational technique, but is dictated by the opportunity of simplified and less time consuming simulations without affecting the physical properties of the remaining atoms as we have verified in few runs of control in which all the ^{4}He atoms are dynamical.

Starting from a well equilibrated run we have locked all the ^{4}He atoms which, according to the radial density profile, have a radial coordinate greater than the minimum between the adsorbed and the third layer, which corresponds to a radius of $r_{\text{lock}}=9.20$ Å (Fig. 1). The 172 adatoms turn out to be arranged in a regular triangular lattice with some defects, induced by the mismatch between a triangular lattice and the size of the adsorbed layer. By locking the atoms of this adsorbed layer we generate an effective static potential for all the other ^{4}He atoms which contains a corrugation contribution due to the locked adatoms, giving a more realistic description of the confinement, even if we lose the zero point motion contribution of the adsorbed atoms. The adatoms are well localized by the strong van der Waals force; by comparing the results with the adsorbed atoms free and those with

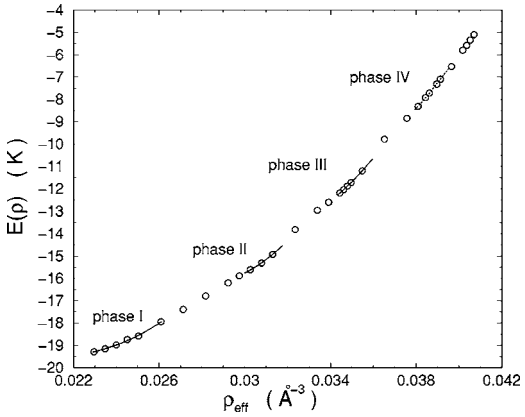

FIG. 2. Energy per particle as function of the effective density ρ_{eff} and phase boundaries from Maxwell construction. The error bars are smaller than the symbols used. The dotted line shows the polynomial fit for the phase IV which cannot be unambiguously characterized. The lowest density of phase IV is obtained by the Maxwell construction with the phase III fit but we are not able to determine its high density boundary as discussed in the text.

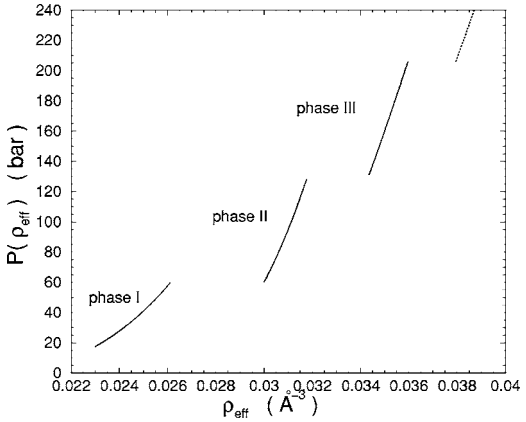

FIG. 3. Pressures as function of the effective density ρ_{eff} as obtained from the polynomial fit of $E(\rho_{\mathrm{eff}})$ and the Maxwell construction. The dotted line is the pressure obtained by the fit of the phase IV.

the adatoms locked we have verified that the contribution of their zero point motion to the microscopic structure of the atoms in the inner region is negligible. Since the locked adatoms do not contribute anymore to the energy and to the other computed quantities of the system, we give our results in terms of effective density of the system ρ_{eff} which is the ratio between the number of free atoms and the effective cylindrical volume defined by radius r_{lock} and height L.

The interactions between atoms are, as usually, explicitly taken into account for pairs with distances up to $L/2$. A tail correction has been added to the energy by computing the contribution to the potential energy for pair distances from $L/2$ to $2L$ in a system four time longer obtained considering four images of our simulation box in the z direction.[29]

III. RESULTS AND DISCUSSION

A. Equation of state and microscopic structure

In Fig. 2 we plot the energy per particle $E(\rho_{\mathrm{eff}})$ as a function of the effective density. The data for $E(\rho_{\mathrm{eff}})$ display some change in the curvature which is below the statistical error of the MC runs. This is a signature of the presence of different phases in the system. It is possible to characterize at least four different phases. For effective densities above 0.036 Å^{-3} it is difficult to identify in an unambiguous way the single phases. Fitting the energy vs density curve with a third-degree polynomial form[22] in restricted range of density we are able to give an estimation of the pressure in the system, reported in Fig. 3. Within the Maxwell construction it is possible to give an indication on the phase coexistence regions, the results are reported in Fig. 2 as solid lines interrupted at coexistence. The transition with the lowest pressure takes place at $P=60$ bar, there is another one at $P=130$ bar and the one at the highest pressure in the studied range is at $P=206$ bar.

At all densities the dynamical atoms arrange themselves in layers around the axis of the cylinder. In our pore the number of layers is three but for effective densities above 0.04 Å^{-3} also the axis of the cylinder is filled. This behavior is shown by the radial density profiles $\rho(r)$ plotted in Fig. 4 for few values of ρ_{eff}; the layered structure of the ^{4}He atoms in the pore is also made evident by Fig. 5 where a snapshot of the coordinates of the helium atoms for a simulation at $\rho_{\mathrm{eff}}=0.04070$ Å^{-3} is shown as an example. Such layered structure is enhanced as ρ_{eff} increases and it is stronger in the more external layers. Therefore for all the considered density range the ^{4}He atoms are arranged in concentric annuli, and this is a characteristic property also of classical fluids in cylindrical narrow pores.[29,30] However the ^{4}He atoms are able to exchange between the different layers as indicated by the nonzero density between the peaks in $\rho(r)$. As we increase the effective density of the system the peaks in the radial density profile become sharper and the minima between adjacent layers become lower, starting from the inert layer. The pressure due to the internal layers tends to compress the external ones toward the pore wall, as indicated by the drift of the position of the peak maxima to bigger radii and greater heights with the increasing effective density. This feature

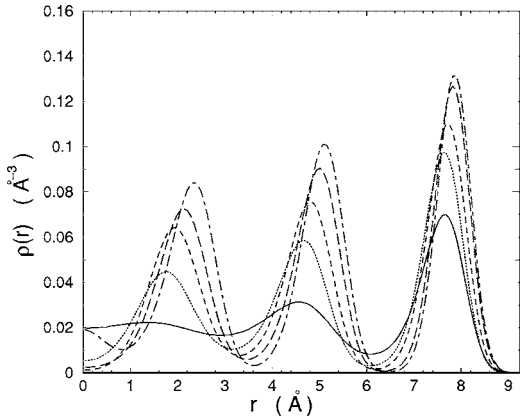

FIG. 4. Radial density profiles for ^{4}He in the pore at different effective densities: $\rho_{\mathrm{eff}}=0.02400$ Å^{-3} (solid), $\rho_{\mathrm{eff}}=0.03026$ Å^{-3} (dotted), $\rho_{\mathrm{eff}}=0.03478$ Å^{-3} (dashed), $\rho_{\mathrm{eff}}=0.03861$ Å^{-3} (long dashed), and $\rho_{\mathrm{eff}}=0.04070$ Å^{-3} (dot-dashed).

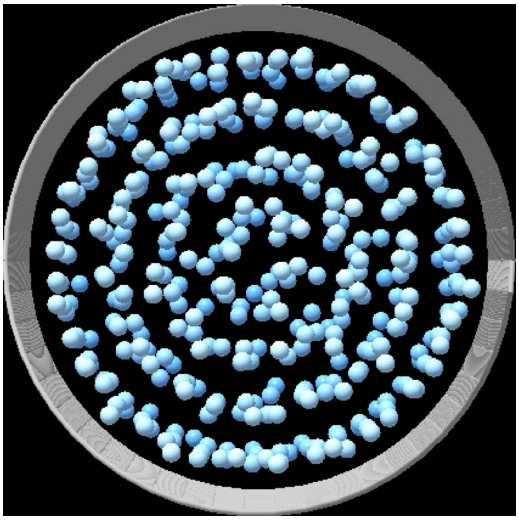

FIG. 5. (Color online) Snapshot along the pore axis of the ^{4}He atom coordinates during a simulation run at $\rho_{\text{eff}}=0.04070$ Å^{-3}.

suggests a layer by layer localization and solidification starting from the more external layer. However the radial density profile is not enough to characterize if and which kind of solid order is present.

In order to characterize the microscopic state of each layer we have computed the static structure factor $S(\mathbf{k})$ separately for each layer. Given the cylindrical symmetry of the container it is convenient to unroll each single layer in a slab and to consider only $\mathbf{k}$ vectors reflecting this symmetry, i.e. using cylindrical coordinates $\mathbf{k}$ has the form $\mathbf{k}=(k_\rho,k_\theta,k_z)$. Periodicity of L in z and of 2π in θ implies that $k_z=2\pi m/L$ and $k_\theta^{(n)}=m'/R_n$ where R_n is the radius of the nth layer and m and m' are integers. No restriction is present on k_ρ which we take to be zero. The static structure factor of the nth layer is then defined as

$$S_n(\mathbf{k})=\left\langle \frac{1}{N_n}\rho_n(\mathbf{k})\rho_n(-\mathbf{k})\right\rangle, \tag{6}$$

where $\rho_n(\mathbf{k})=\Sigma_{j=1}^{N_n}\exp(i\mathbf{k}\cdot\mathbf{r}_j)$ with $\mathbf{r}=(r,\theta,z)$, $\mathbf{k}=(0,k_\theta,k_z)$ and N_n is the number of particles in the nth layer. In order to improve the analysis of the results obtained by the calculation of the static structure factor we have computed also the layer density $\rho_n(\theta R_n,z)$. In Figs. 6–8 we report, for different effective densities, our results for $S_n(\mathbf{k})$ and $\rho_n(\theta R_n,z)$ for the first, second and third layer, respectively.

We start the discussion with the first layer, the outermost dynamical one. From the static structure factor in Fig. 6(a) it is evident that for $\rho_{\text{eff}}=0.02400$ Å^{-3}, which falls in phase I, the first layer is still liquid, even if $S_1(\mathbf{k})$ has two striking peaks. Looking at the contour plot for the planar density $\rho_1(\theta R_1,z)$ reported in Fig. 6(b) it is clear that this liquid layer has a modulation along the z direction and this modulation turns out to be in phase with the density modulation of the adsorbed (0th) layer. It should be noticed that the modulation is slightly tilted away from the z direction by an angle of about 2°. This is shown also in the k space, the sharp modulation peak of $S_1(\mathbf{k})$ has, in fact, a nonzero k_θ component. This effect is present also in the inert layer where the lattice axis is tilted away from the z direction by the same angle and is common in all the solid layers. This is due to a mismatch between the lattice constant of the helium lattice with the circumferences of the layers. By increasing the effective density the atoms in the first layer start to arrange themselves in a triangular lattice, as shown by the six sharp peaks in $S_1(\mathbf{k})$ [Figs. 6(c), 6(e), and 6(g)]. The heights of these peaks are not the same for all of them except for the highest density, the ones along the z direction are higher than the other four peaks. Looking at the correspondent contour plots, this can be interpreted as a triangular solid with some defects which are more localized in the z direction than in the tangential one. At $\rho_{\text{eff}}=0.03860$ Å^{-3} the solidification is complete: the peaks in $S_1(\mathbf{k})$ have all the same height [Fig. 6(g)] and in the contour plot [Fig. 6(h)] the atoms appear well localized around equilibrium positions.

We discuss now the second layer. $S_2(\mathbf{k})$ is isotropic in k_θ and the dependence on k_z is typical of a liquid in phase I and II [see Fig. 7(a)]. At $\rho_{\text{eff}}=0.03478$ Å^{-3}, in phase III, peaks start to grow from the liquid background [Fig. 7(c)] and this can be interpreted as a solid with some mobile defects as shown by the density contour plot in Fig. 7(d). Increasing the effective density the solid order becomes more evident, and the solidification is complete at $\rho_{\text{eff}}=0.04070$ Å^{-3}, as shown in Figs. 7(g) and 7(h).

Since the third layer is always liquid up to $\rho_{\text{eff}}=0.03548$ Å^{-3}, we can interpret the phase transition between the phase I and II as due to the solidification of the first layer, while the one between phase II and III as due to the solidification of the second layer. Then in phase I all the system is in the liquid phase, in phase II the first layer becomes solid while the other two layers remain liquid and in phase III only the third layer is still liquid. It is interesting to note that the solidification of both the first and the second layer occurs at the same areal density of about 0.09 Å^{-2}. This areal density is substantially larger of the freezing density found in a pure 2D system[31] which is $\rho_{2D}^{freeze}=0.0721$ Å^{-2}.

For ρ_{eff} higher than 0.03548 Å^{-3} it is not possible to unambiguously characterize the microscopic phase of the third layer. At $\rho_{\text{eff}}=0.03548$ Å^{-3} the areal density of the third layer is equal to the freezing value 0.09 Å^{-2} of the other two layers, then we might expect it to become solid (phase IV). On the other hand the static structure factor $S_3(\mathbf{k})$ shows six peaks for the third layer only at $\rho_{\text{eff}}=0.04070$ Å^{-3}, as shown in Fig. 8. This can be due to a commensuration problem between the lattice parameters and the circumference of the layer as well as to the presence of some free space in the center of the pore. There are at least three reasons why it is difficult a full characterization of the phase diagram at the highest densities of our computation, i.e., the range of effective densities where the third layer is solid and the coexistence region with the phase III. First, the ^{4}He atoms involved in this phase transition are about 25, significantly less than the 115 and 65 particles involved in the previous two phase transitions, respectively. As a consequence the signature of this phase transition in the diagram of $E(\rho_{\text{eff}})$ reported in Fig. 2 is smaller than the previous ones, and it can be masked by the uncertainty in the optimization of the variational param-

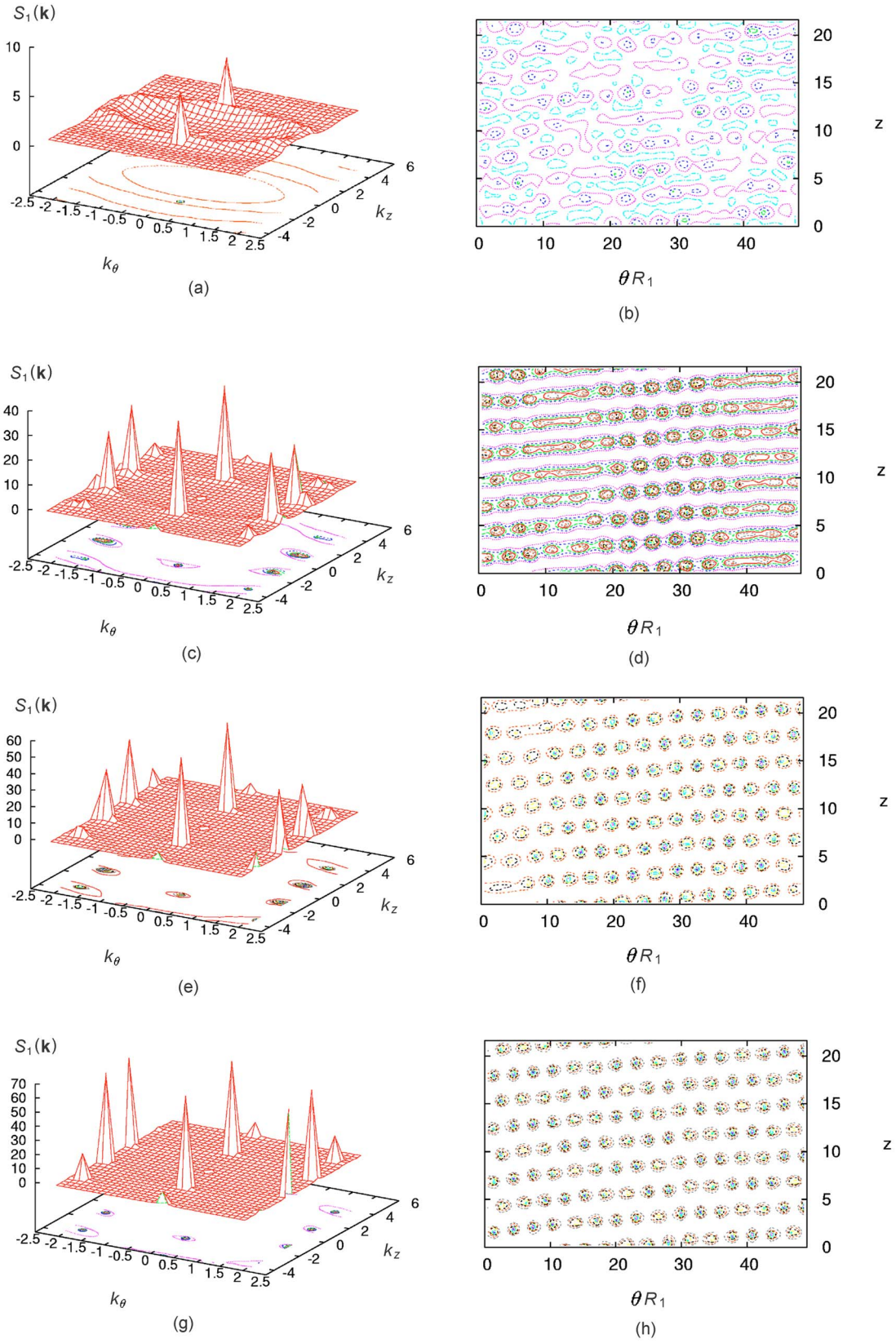

FIG. 6. (Color online) Static structure factors $S_1(\mathbf{k})$ [(a),(c),(e),(g)] and contour plots for the planar density $\rho_1(\theta R_1, z)$ [(b),(d),(f),(h)] for the first layer at different effective densities: ρ_{eff}=0.02400 Å^{-3} [(a),(b)], 0.03026 Å^{-3} [(c),(d)], 0.03478 Å^{-3} [(e),(f)], and 0.03860 Å^{-3} [(g),(h)].

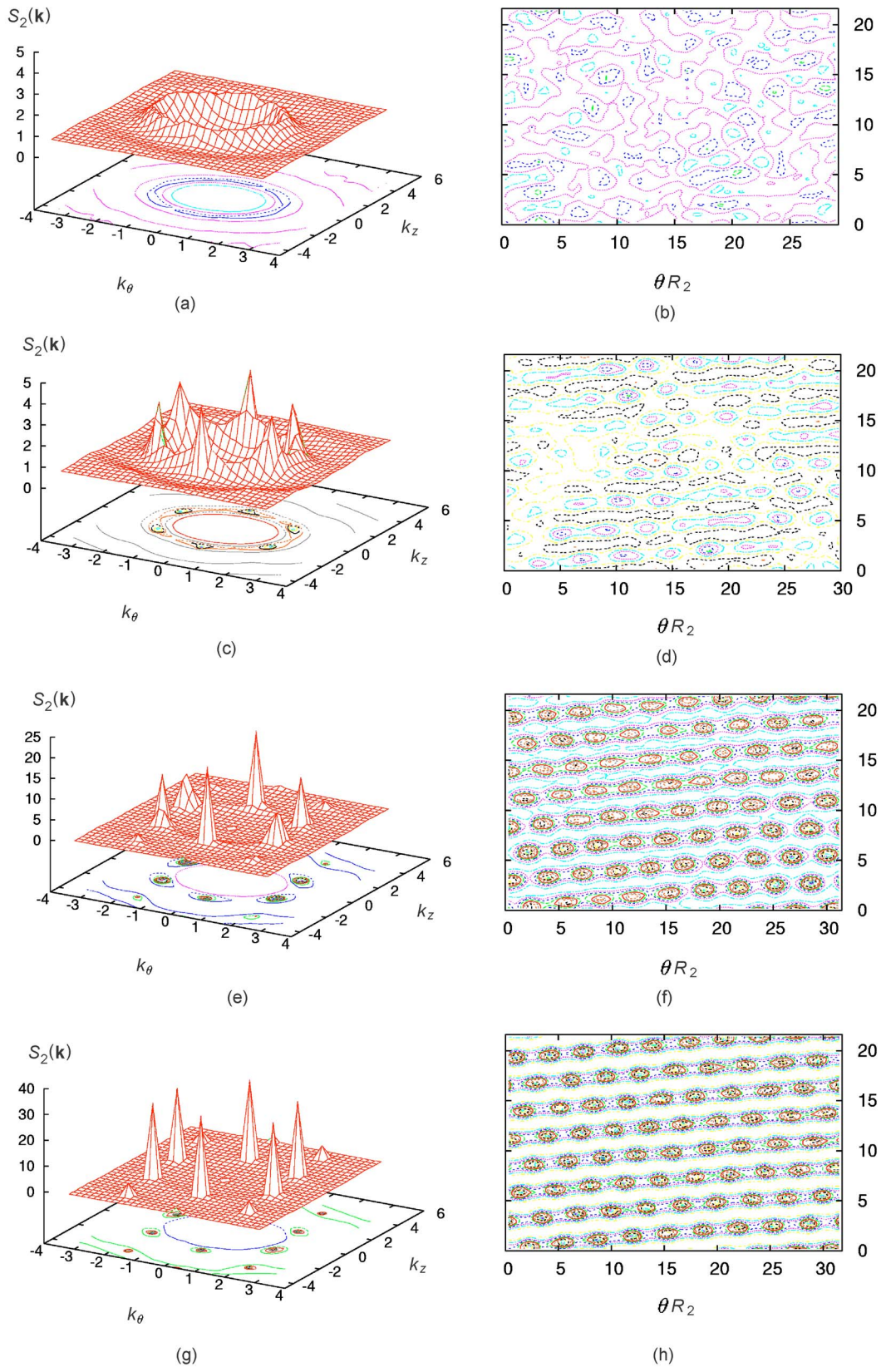

FIG. 7. (Color online) Static structure factors $S_2(\mathbf{k})$ [(a),(c),(e),(g)] and contour plots for the planar density $\rho_2(\theta R_2, z)$ [(b),(d),(f),(h)] for the second layer at different effective densities: ρ_{eff}=0.03026 Å^{-3} [(a),(b)], 0.03478 Å^{-3} [(c),(d)], 0.03860 Å^{-3} [(e),(f)], and 0.04070 Å^{-3} [(g),(h)].

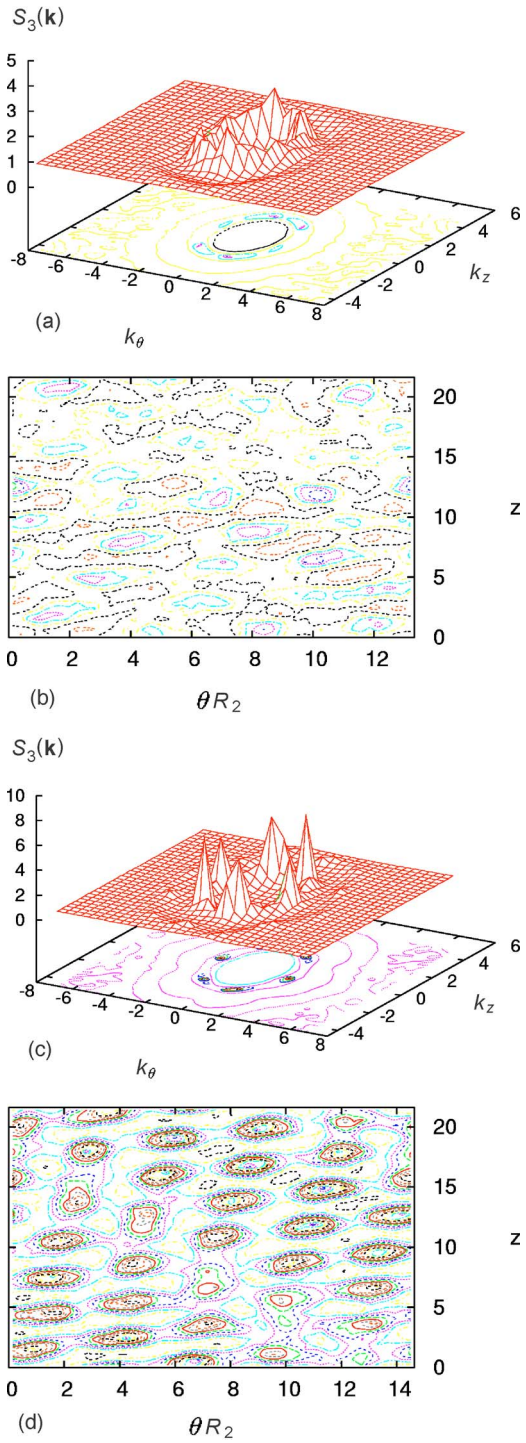

FIG. 8. (Color online) Static structure factors $S_3(\mathbf{k})$ [(a),(c)] and contour plots for the planar density $\rho_3(\theta R_3, z)$ [(b),(d)] for the third layer at $\rho_{\text{eff}}=0.03860$ Å^{-3} [(a),(b)] and $\rho_{\text{eff}}=0.04070$ Å^{-3} [(c),(d)].

eters. Moreover, our choice for the pseudopotentials in the wave function can be less accurate for so high density solid. Furthermore, at the highest ρ_{eff} the system is undergoing a structural transition from a configuration with three layers to one with three layers plus the filled center; this can be seen for $\rho_{\text{eff}}=0.04070$ Å^{-3} in Fig. 4 where also the cylinder axis starts to be populated by ^{4}He atoms. Therefore at such high densities it is dubious the application of the Maxwell construction and we give only some qualitative indications on the behavior and on the properties of the system.

In order to obtain more information on the kind of solid order in our system we have computed also the coordination number and the angular probability distribution $P(\theta,\phi)$ for each layer. The coordination number of the nth layer has been computed as the average of the number of atoms which fall into a sphere of radius r_{min} centered on a ^{4}He atom in the considered layer. The radius r_{min} is fixed to the position of the first minimum in the pair distribution function $g(r)$, then the coordination number gives the number of first neighbors for each He atom in the nth layer. We find that in phase III, when the first and the second layer are solid, the coordination number for the first layer is very close to 12, the value of a close packed solid. For the second layer this become true in phase IV and for the third layer the coordination number becomes close to 12 only at $\rho_{\text{eff}}=0.04070$ Å^{-3}. The kind of close packed solid can be determined by studying the angular distribution of the position of the first neighbors. This is done by analyzing the angular probability distribution $P_n(\theta,\phi)$ for each layer, which comes from a four body correlation function.[20,21] $P_n(\theta,\phi)$ is computed as follows: an atom in the nth layer is chosen to fix the origin of a new reference frame, two of its first neighbors, in the same layer, are chosen to fix the direction of the z axis and the xz plane respectively, and then the angular coordinates (θ,ϕ) in this new reference frame of the remaining first neighbors are recorded. The kind of crystalline order, if any, is characterized by the position of the peaks in the plot of $P_n(\theta,\phi)$. We find that, for effective density greater than 0.03432 Å^{-3} (phase III), $P_1(\theta,\phi)$ is compatible with an hcp lattice. This suggests that the ^{4}He atoms arrange themselves in the layer as in the basal planes of an hcp crystal. For ρ_{eff} greater than 0.038 Å^{-3}, $P_2(\theta,\phi)$ shows a structure which resembles that of an hcp lattice, but substantial distortions are present. This is probably due to the curvature of the second layer and to the stronger one of the third layer, whose atoms are involved in the computation. For the same reason $P_3(\theta,\phi)$ has not an hcp structure even at $\rho_{\text{eff}}=0.04070$ Å^{-3}. Indeed, because of the presence of mobile defects in the third layer, as shown by the $\rho_3(\theta R_3, z)$ contour plot in Fig. 8(d), the peaks in $P_3(\theta,\phi)$ are smeared out resulting in a smooth surface from which no information on the angular coordination between atoms can be extracted.

The major features that emerge from our simulations are that the solidification takes place starting from the pore wall and that the system does not enter in a crystalline ordered phase (all the layers solid) up to very high pressures. A number of models concerning the solidification of fluids in restricted geometries, with different hypotheses and previsions, have been developed in the past years.[3,28,32] The first model predicted the nucleation of solid at the pore wall thanks to the localization induced by the strong van der Waals forces[32] with a resulting lower solidification pressure than the bulk one. But from the experimental observation[1–3] it is observed that an extra-pressure of about 15 bar over the bulk one is necessary for solidification of ^{4}He in Vycor. Today, the widely accepted mechanism for solidification in pores is that the solid nucleates within the liquid region at the center of the pore[3] and an extra pressure ΔP over the freezing pressure

in the bulk (25 bar for ^{4}He) is needed for solidification of ^{4}He in a porous material. In fact, due to the irregular nature of the pore surfaces, the ^{4}He atoms are readily localized in a nonsuperfluid amorphous layer which discourages the formation of crystallites at the pore surface; indeed, a solid which grows on a substrate is strongly strained if the lattice constants or the symmetry of the solid and the substrate do not match each other.

Some of these features are also encountered for classical particles in porous material.[30] They are essentially due to the cylindrical geometry: in fact, although freezing transition occurs in slit pores for all pore widths, down to widths that accommodate just one layer of adsorbate, the additional confinement of the cylindrical pore makes it harder for the atoms to arrange themselves on the appropriate lattice points. Then for classical particles the freezing pressures (temperatures) are in general higher (lower) for cylindrical than for slit pores of the same porous material and pore width.[30] Both simulations and experimental studies[30] have shown that for pore diameters below about 20σ (where σ is the diameter of the molecule) only partial freezing occurs, with a mixture of 3D microcrystals and amorphous domains, while for still smaller pores even partial crystallization is not observed. These studies suggest that the lower pore diameter below which no crystal domain occurs is roughly 12σ for silica materials. Then, taking $d=2.14$ Å as the effective ^{4}He atom diameter,[33] we obtain a value of about 25.7 Å as lower bound for the critical pore diameter under which no crystallization should occur. Obviously we can expect that to localize ^{4}He atoms in lattice positions turns out to be even more difficult than for a classical fluid, due to quantum effects.

Experimentally it is still not known, for ^{4}He, if the solid in the center of the pores is bulklike or not, but recent neutron scattering results for ^{4}He in a larger diameter Gelsil (44 Å) are compatible with an hcp solid.[6] However there must be a transition region between the amorphous layers adsorbed at the pore wall and the crystalline solid in the center. This transition region is supposed to be responsible[28] of the "anomalies" in restricted geometry, as the smaller molar volume change in the liquid-solid phase transition of ^{4}He in Vycor than in the bulk.[1] Moreover, this transition region results in a liquid layer which is found to be responsible for a superfluid response of ^{4}He at a pressure of 62 bar in a recent PIMC simulation performed in a slit pore geometry for Vycor.[10] The thickness t of this transition region is estimated by neutron scattering to be of the order of 10 Å for D_2 in Vycor and it is expected to be quite larger for quantum solids as hydrogen or helium.[28] Since t is related to the pore radius (if R is very large the effect of the wall curvature is negligible and the solid is slightly strained at the pore wall), we might argue that our $R=13$ Å nanopore cannot stand with a bulklike solid in its center because the transition region exhausts the whole available volume. In fact, we have performed a computation in which we have filled the effective volume of our pore with the ^{4}He atoms in the initial configuration corresponding to an hcp solid for different effective densities. We find that just 10^5 Monte Carlo steps are enough to completely destroy this kind of solid order and to give rise to the layered structure even when the length of the pore is chosen to be commensurate with the c lattice parameter of the hcp crystal. It would be interesting to perform microscopic simulations increasing the pore radius in order to find the diameter at which the nucleation of solid ^{4}He from the central liquid region takes place.

We conclude that our narrow pore accommodates only the "transition region" which presents a strong layered structure, and very high pressures are requested to induce solid order in the layers. It appears that a major role on the difficulty of the layers to reach a crystalline order is due to a commensuration effect in the tangential direction, which is imposed by the pore radius (i.e., by a model parameter and not by the chosen size of the simulation box). This kind of commensuration problem is surely encountered by ^{4}He in a real tortuous and irregular porous material of small diameter like in Gelsil. However we find that the solidification of the layers takes place when the areal density reaches the value 0.09 Å^{-2}. Since the lattice parameter for a triangular lattice at the areal density of 0.09 Å^{-2} is commensurate with our standard pore length $L=21.62$ Å, we have performed simulations with different L, both larger and smaller of our standard L, for a number of effective densities, in order to verify the presence of size effects on the microscopic phase of the layers induced by the choice of L. In general we find that the microscopic structure remains unchanged, moreover the static structure factor shows solid order always only for areal density greater than 0.09 Å^{-2}. We conclude that the small value of L should not affect in a substantial way the pressures of the layer by layer transitions.

In order to exclude effects due to the geometry of the peculiar locked configuration of the inert layer, we have also performed simulations with the same pore length but locking the adatoms in different configurations. We have found no substantial differences in the microscopic structure of the system; this is an expected result since we have already verified that the zero point motion of the adatoms has a negligible effect on the microscopic structure of the inner layers.

B. Condensate fraction

The condensate fraction is obtained by computing the one-body density matrix $\rho_1(\mathbf{r},\mathbf{r}')$ which represents the probability amplitude of destroying a particle in $\mathbf{r}$ and creating one in $\mathbf{r}'$. Its Fourier transformation (FT) represents the momentum distribution. In first quantization the one-body density matrix is given by the overlap between the normalized many-body ground state wave function $\Psi(R)$ and $\Psi(R')$, where the configuration $R'=(\mathbf{r}',\mathbf{r}_2,\ldots,\mathbf{r}_N)$ differs from $R=(\mathbf{r},\mathbf{r}_2,\ldots,\mathbf{r}_N)$ only by the position of one of the N atoms in the system. If $\Psi(R)$ is translationally invariant, ρ_1 only depends on the difference $\mathbf{r}-\mathbf{r}'$

$$\rho_1(\mathbf{r}-\mathbf{r}')=N\int d\mathbf{r}_2\ldots d\mathbf{r}_N\Psi^*(R)\Psi(R'). \tag{7}$$

The Bose-Einstein condensate fraction n_0 is equal to the limit of $\rho_1(\mathbf{r}-\mathbf{r}')$ for $\mathbf{r}-\mathbf{r}'\to\infty$. In fact, if ρ_1 has a nonzero plateau at large distance, the so called off-diagonal long-range order (ODLRO), its FT contains a Dirac delta function, which indicates a macroscopic occupation of a single momentum state, i.e., BEC.

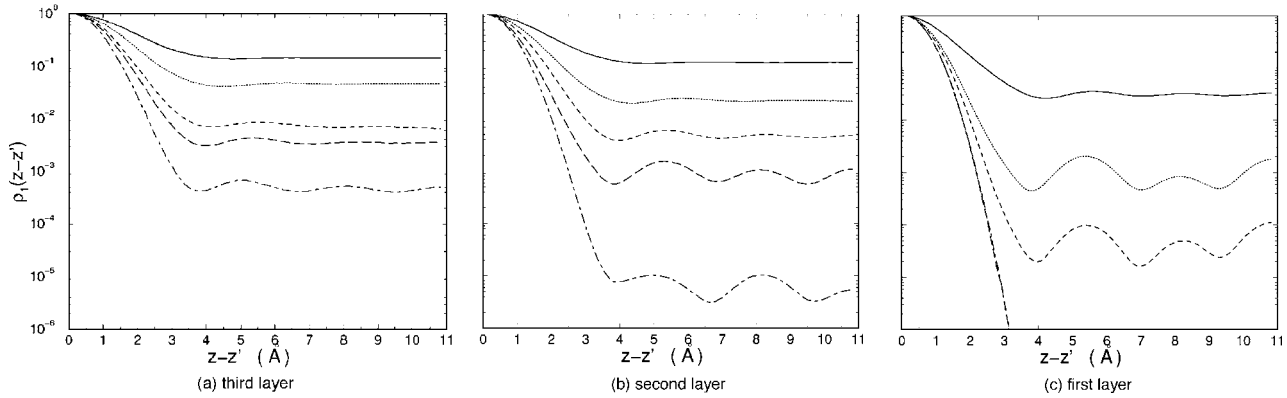

FIG. 9. One-body density matrix $\rho_1(z-z')$ along the axial direction in each layer at some different effective densities [ρ_{eff} =0.02400 Å^{-3} (solid line), 0.03026 Å^{-3} (dotted), 0.03478 Å^{-3} (dashed), 0.03861 Å^{-3} (long dashed), and 0.04070 Å^{-3} (dot dashed)].

Because of the cylindrical geometry of our system we are allowed to take the limit to large distances only along the z direction. By taking the points $\mathbf{r}$ and $\mathbf{r}'$ at the same distance $r_\perp$ from the pore axis and taking $r_\perp$ equal to the position r_n of the maximum of the nth layer obtained from the radial density profile, we have computed $\rho_1(z-z')$ separately for each layer. In order to improve the statistics we average in the θ direction for symmetry. Our results for the one-body density matrix are reported in Fig. 9. The most important feature is that ODLRO is present in our system for a very large pressure range. Even at pressure of order 250 bar the inner two layers have a small but finite condensate. In Table II we report the global condensate fraction given by the weighted sum of the condensate fractions in each layer.

The oscillations in the long distances tail of $\rho_1(z-z')$ reflect a crystalline order of the layer; in fact, the positions of the maxima turn out to be located at integer multiples of the lattice spacing in the z direction. Then there is a finite n_0 even when the layer is in the solid phase. The presence of BEC in a solid system is not unexpected: recently, with the SWF technique, we have found a nonzero condensate fraction both in perfect and in defected bulk solid helium.[12,34] We know that in the solid layers in the pores some defects are present, such as vacancies, as revealed by the layer contour plot in Figs. 6–8, and defects are known to enhance the delocalization of the atoms favoring BEC.[12,34] This explains the large value of n_0 in the present case compared to the bulk case at similar densities. In addition we find that the oscillations in the tail of $\rho_1(z-z')$ are registered with the crystalline lattice of the layer and not dephased by half lattice parameter like in bulk crystalline ^{4}He. Therefore in the present case the dominant contribution to the value of n_0 is due to disorder rather than to the vacancy-interstitial pairs creation due to the zero point motion of the ^{4}He atoms as is the case of bulk.[12]

We find, as expected, that the condensate fraction n_0 in each layer decreases with the increasing density, and for the first layer it is vanishing small [Fig. 9(c)] at the highest densities of our computation when full localization of the ^{4}He atoms in the layer is achieved. This happens when the coverage of the first layer is about 0.116 Å^{-2}, which corresponds to a density of 0.045 Å^{-3} in bulk solid ^{4}He and to a pressure of 630 bar.[27] At ρ_{eff}=0.03478 Å^{-3}, which corresponds to an areal density of 0.110 Å^{-2} and a lattice parameter equal to the value of bulk ^{4}He at a pressure of 376 bar, this first layer still has a condensate fraction of the order 3×10^{-5}.

From the experimental point of view, the reduction of the superfluid density ρ_s with increasing pressure, observed for ^{4}He in Vycor, was attributed to the blockade of pores by solid ^{4}He.[3] This picture has been recently proposed also in a 44 Å diameter Gelsil study[6] where the disappearance of the roton signal from the excitations spectrum is interpreted as a signature of a complete solidification of the ^{4}He in the pores. Moreover an anomalous continuous suppression to 0 K of the critical temperature T_c for the transition to the superfluid phase for ^{4}He in Gelsil has been recently reported.[5] The small size and disorder of the pore structure may be responsible for the reduction in T_c and ρ_s because ^{4}He atoms can localize in the narrowest pores[5,6] and solid plugs can be present in the largest one, or in the regions where two or more pores connected each other, hindering the superfluid flow. This means that the possibility of positional exchanges between ^{4}He atoms, needed for the superfluidity,[35] is greatly reduced.

Because of the presence of ODLRO, our solid layers are nonclassical solids, but if this feature implies a superfluid response of the system is not clear yet. For example, for the interacting Bose gas in presence of strong disorder it is possible to reach a state in which the superfluid density is zero but the condensate fraction is still finite.[15]

IV. CONCLUSIONS

We have studied the T=0 K phase diagram of ^{4}He filling a silica porous material modeled by a single smoothed 13 Å radius nanopore via the variational SWF technique. At all the considered densities the ^{4}He atoms arranges themselves in concentric annuli giving rise to a distinct layered structure. The properties of the adsorbed layer, which is always solid in the studied density range, are found to be independent on the total density of the system, then, locking the position of the ^{4}He atoms, we have treated this inert layer as a part of the substrate. We find that, by increasing the density, the solidification takes place layer by layer starting from the layer closest to the inert one. Due to the small size of the pore a bulklike solid is not allowed to nucleate in the central liquid region. The phase diagram has at least four phases. In the

TABLE II. Global condensate fraction in our 13 Å radius pore obtained by summing each layer condensate fraction weighted with the number of particle in the correspondent layer and normalized with the total (free plus locked) number ^{4}He atoms in the system, n_{0t}, and with the number of free ^{4}He atoms, n_{0f}. The corresponding pressure P is also reported.

ρ_{eff} (Å^{-3})	P (bar)	n_{0t}	n_{0f}
0.02400	7.7	$(2.93\pm0.03)\times10^{-2}$	$(6.6\pm0.1)\times10^{-2}$
0.03026	68.3	$(5.8\pm0.1)\times10^{-3}$	$(1.15\pm0.02)\times10^{-2}$
0.03478	150.3	$(1.84\pm0.03)\times10^{-3}$	$(2.20\pm0.05)\times10^{-3}$
0.03861	$\simeq$230	$(3.8\pm0.3)\times10^{-4}$	$(3.7\pm0.5)\times10^{-4}$
0.04070	$\simeq$330	$(3.7\pm0.3)\times10^{-5}$	$(6.4\pm0.5)\times10^{-5}$

density range under study, below a pressure of 60 bar the whole dynamical system is in a stratified liquid phase and only above 200 bar solidification of all the layers is completed. In the intermediate pressure range there is partial freezing layer by layer. In our idealized model we find sharp phase transitions. In a real porous media we might expect some kind of smoothing out of the transitions due to wall roughness and deviation from a regular cylindrical geometry. However, the fact that the inert layer does not play a significant role in the phase behavior of the inner layers suggests that small asperities in the wall will be compensated by the inert layer and the basic progression of solidification inward from the wall should be found also in real porous media.

We find also that a nonzero condensate fraction is always present in the studied density range, even when all the layers are in the solid phase. This condensate fraction decreases with increasing density but it is not suppressed even for pressures up to 270 bar. From the analysis of the oscillations in the plateau of the one-body density-matrix we recognize the presence of defects such as vacancies as the main microscopic origin of the condensate fraction in the solid layers.

It seems to us important to underline that the size distribution of the real porous glasses makes difficult a detailed comparison between our single pore model results with the experimental ones. On the other hand experiments with different porous materials give what we consider some contradictory results. The observed freezing pressure in 40 Å diameter Gelsil of 40 bar,[6] determined by the disappearance of the roton signal from the excitations spectrum and by the analysis of the Braggs peaks, is lower than the believed Vycor freezing pressure (45 bar) even if the pore size is smaller than the nominal size of Vycor pores (70 Å). This is not what we observe in our 26 Å diameter pore and what is expected by the widely accepted mechanism for solidification in pores[3,28] which predicts that the extra-pressure over the bulk freezing pressure necessary to the solidification is inversely proportional to the radius of the pore. Moreover PIMC simulations of ^{4}He in a slit pore Vycor geometry show the presence of a liquid layer also at pressures of 62 bar.[10] The disappearance of the rotons with the increasing pressure can be due not only to the solidification of the whole system, but also to a modification of the excitations spectrum induced by the particularly confined geometry of Gelsil. It would be interesting to extend our study to investigate the excitations by means of the SWF technique. This would be relevant especially for the additional information on the superfluid behavior that can be deduced by the spectrum.

ACKNOWLEDGMENTS

This work was supported by the INFM Parallel Computing Initiative and by the Mathematics Department "F. Enriques" of the Università degli Studi di Milano.

[1] J. R. Beamish, A. Hikata, L. Tell, and C. Elbaum, Phys. Rev. Lett. **50**, 425 (1983); E. D. Adams, K. Uhlig, Yi-Hua Tang, and G. E. Haas, Phys. Rev. Lett. **52**, 2249 (1984).
[2] D. N. Bittner and E. D. Adams, J. Low Temp. Phys. **97**, 519 (1994).
[3] Cao Lie-Zhao, D. F. Brewer, C. Girit, E. N. Smith, and J. D. Reppy, Phys. Rev. B **33**, 106 (1986).
[4] J. D. Reppy, J. Low Temp. Phys. **87**, 205 (1992); M. H. W. Chan, M. Mulders, and J. D. Reppy, Phys. Today **49**(8), 30 (1996).
[5] K. Yamamoto, H. Nakashima, Y. Shibayama, and K. Shirahama, Phys. Rev. Lett. **93**, 075302 (2004).
[6] J. V. Pearce, J. Bossy, H. Schober, H. R. Glyde, D. R. Daughton, and N. Mulders, Phys. Rev. Lett. **93**, 145303 (2004).
[7] M. C. Gordillo and D. M. Ceperley, Phys. Rev. Lett. **85**, 4735 (2000).
[8] V. Apaja and E. Krotscheck, Phys. Rev. B **67**, 184304 (2003); Phys. Rev. Lett. **91**, 225302 (2003).
[9] D. E. Galli and L. Reatto, J. Low Temp. Phys. **136**, 343 (2004).
[10] S. A. Khairallah and D. M. Ceperley, physics/0502039.
[11] A. F. Andreev and I. M. Lifshitz, Sov. Phys. JETP **29**, 1107 (1969); G. V. Chester, Phys. Rev. A **2**, 256 (1970); A. J. Leggett, Phys. Rev. Lett. **25**, 1543 (1970).
[12] D. E. Galli, M. Rossi, and L. Reatto, Phys. Rev. B **71**, 140506(R) (2005).
[13] E. Kim and H. W. Chan, Nature (London) **427**, 225 (2004).
[14] E. Kim and H. W. Chan, Science **305**, 1941 (2004).
[15] G. E. Astrakharchik, J. Boronat, J. Casulleras, and S. Giorgini, Phys. Rev. A **66**, 023603 (2002).
[16] S. Vitiello, K. Runge, and M. H. Kalos, Phys. Rev. Lett. **60**, 1970 (1988).
[17] F. Pederiva, A. Ferrante, S. Fantoni, and L. Reatto, Phys. Rev. Lett. **72**, 2589 (1994).
[18] S. Moroni, D. E. Galli, S. Fantoni, and L. Reatto, Phys. Rev. B **58**, 909 (1998).
[19] D. E. Galli and L. Reatto, Physica B **284–288**, 345 (2000).
[20] M. Buzzacchi, D. E. Galli, and L. Reatto, Phys. Rev. B **64**, 094512 (2001); D. E. Galli, M. Buzzacchi, and L. Reatto, J. Chem. Phys. **115**, 10239 (2001).
[21] M. Rossi, M. Verona, D. E. Galli, and L. Reatto, Phys. Rev. B **69**, 212510 (2004).
[22] T. MacFarland, S. A. Vitiello, L. Reatto, G. V. Chester, and M. H. Kalos, Phys. Rev. B **50**, 13577 (1994).

[23] R. A. Aziz, V. P. S. Nain, J. S. Carley, W. L. Taylor, and G. T. McConville, J. Chem. Phys. **70**, 4330 (1979).
[24] G. Stan, M. J. Bojan, S. Curtarolo, S. M. Gatica, and M. W. Cole, Phys. Rev. B **62**, 2173 (2000).
[25] G. Vidali, G. Ihm, H. Y. Kim, and M. W. Cole, Surf. Sci. Rep. **12**, 133 (1991).
[26] L. D. Gelb and K. E. Gubbins, Langmuir **14**, 2097 (1998).
[27] A. Driessen, E. van der Poll, and I. F. Silvera, Phys. Rev. B **33**, 3269 (1986).
[28] M. Schindler, A. Dertinger, Y. Kondo, and F. Pobell, Phys. Rev. B **53**, 11451 (1996).
[29] A. Z. Panagiotopoulos, Mol. Phys. **62**, 701 (1987).
[30] R. Radhakrishnan, K. E. Gubbins, and M. S. Bartkowiak, J. Chem. Phys. **116**, 1147 (2002) and references therein.
[31] P. A. Whitlock, G. V. Chester, and M. H. Kalos, Phys. Rev. B **38**, 2418 (1988).
[32] J. G. Dash, Phys. Rev. B **25**, 508 (1982).
[33] M. H. Kalos, D. Levesque, and L. Verlet, Phys. Rev. A **9**, 2178 (1974).
[34] D. E. Galli and L. Reatto, J. Low Temp. Phys. **124**, 197 (2001).
[35] E. L. Pollock and D. M. Ceperley, Phys. Rev. B **36**, 8343 (1987).